RESERVE THIS SPACE

# Atomistic Simulations of Plasmon Mediated Photochemistry

**Author: Yu Zhang[1*], Tammie Nelson[1], Sergei Tretiak[1,2]**

**1. Theoretical Division, Los Alamos National Laboratory, Los Alamos, NM, 87545, US**

**2. Center for Integrated Nanotechnologies, Los Alamos National Laboratory, Los Alamos, NM, 87545, US**

*Email: zhy@lanl.gov

Abstract: Chemical reactions mediated by localized surface plasmons have been identified as a viable pathway for efficiently converting solar energy to chemical energy. The excitation and decay of plasmons have found applications in catalysis via different mechanisms. Especially, recent reports demonstrated that the hot charge and energy carriers generated from plasmon decay in nanoparticles could transfer to attached molecules and drive photochemistry, which was previously thought to be impossible. In recent work, we have computationally explored the atomic-scale mechanism of a plasmonic hot-carrier-mediated chemical process, $H_2$ dissociation. Numerical simulations demonstrate that, after photoexcitation, hot carriers transfer to the antibonding state of the $H_2$ molecule from the nanoparticle, resulting in a

RESERVE THIS SPACE

repulsive-potential-energy surface and $H_2$ dissociation. This process occurs favorably when the molecule is close to a single nanoparticle. However, if the molecule is located at the center of the spatial gap in a plasmonic dimer, dissociation is suppressed due to sequential charge transfer, which efficiently eliminates occupation in the antibonding state and, in turn, reduces dissociation. An asymmetric displacement of the molecule in the gap breaks the symmetry and restores dissociation when the additional charge transfer becomes significantly suppressed. Thus, these models demonstrate the possibility of structurally tunable photochemistry via plasmonic hot carriers.

## Introduction

Surface plasmon polaritons (SPPs) and localized surface plasmon resonances (LSPRs) are collective oscillations of electrons in conductors excited by electromagnetic modes that are confined to the conductor–dielectric interfaces [1-3]. LSP of a metallic nanoparticle (NP) can be excited by illumination, which triggers a set of complex dynamical processes, including the localization of strong optical near field, re-emission of a photon, hot-carrier generation, ejection and relaxation of hot-carriers, these important processes are depicted in Figure 1. Due to the LSP resonance in metallic nanostructures, light absorption can be significantly enhanced, resulting in strong light concentration in the near field around the nanostructure interfaces as illustrated by Figure 1a [4-5], which enables efficient spatial control of charge and energy fluxes in a variety of applications. The strong light enhancement has been used in many surface-enhanced processes, including surface-enhanced Raman spectroscopy (SERS) [6,7], photochemistry on surfaces [8], fluorescence [9], and solar energy conversion [10]. Recent studies also found the strong light enhancement could be employed as a driving force in chemical reactions. The direct intramolecular excitation from the HOMO to the LUMO of molecules can be induced resonantly by the LSP with the same energy as the HOMO-LUMO gap, as shown by the red arrow of Figure 1(f) [11]. Moreover, when the molecules are adsorbed on metals, their optical energy gap can be reduced because of the hybridization between the molecular orbitals and metal states, thus providing excitation pathways accessible by LSP.

However, surface plasmons suffer from significant dissipation [12]. Plasmon resonances in nanostructures can be damped radiatively by emitting a

photon or non-radiatively through the creation of hot electron-hole pairs via Landau damping, resulting in a swarm of hot electrons and holes (Figure 1b) [13]. Landau damping is a pure quantum mechanical process in which a quantum plasmon is transferred into a single electron-hole pair. After generation from the plasmon decay, the hot electrons will quickly redistribute the energy among many lower-energy electrons, and the temperature of the conduction electrons increases due to electron-electron scattering processes (Figure 1c). The additional energy of the lower-energy electrons is then dissipated via electron-phonon scattering, resulting in local heating (raising the lattice temperature). Similar dynamics of this process for extended surfaces has been described by a two-temperature model [14]. Finally, the heat is transferred to the surroundings of the metallic structure by thermal conduction (Figure 1d). Even through ultrafast hot-carrier generation dominates the energy dissipation of SPPs [15] and limits plasmonics applications due to the short plasmon lifetime, several recent efforts have proposed possible scenarios of hot carrier extraction before dissipation takes place [16-19]. This has stimulated the application of hot carriers to several branches of applied physics, chemistry, and materials and energy sciences [19-29]. Since different processes of the plasmon decay take place on different timescales, the energetic electron-hole pairs and heating effects can be used by the molecules as stimuli for driving chemical reactions in photocatalysis via different mechanisms [30]. This process is different compared to common photochemical reactions occurring in natural systems, including the photoisomerization in vision [31], photosynthesis in plants [32], and gating of certain ion channels [33]. Plasmon-driven photochemistry has received increasing attention in recent years for its potential to overcome the intrinsic limitations of conventional semiconductor photocatalysis. Recent studies have shown that the hot carriers generated in plasmonic structures can be transferred to adjacent electron acceptors, inducing such photochemical processes as diatomic $H_2$, $O_2$, and $N_2$ dissociation [34-41,42], proton reduction [43], water splitting [44-48], artificial photosynthesis [49], and hydrocarbon conversion [50]. The unique feature of metallic NPs, namely that their optical properties are tunable over a wide spectral range via changes in size, shape, and composition, makes these systems appealing for plasmon-induced chemistry [5]. The NPs used in photochemistry are typically gold spheres with sizes as small as several nanometers. It has been demonstrated that the LSP can not only enhance reaction efficiency by its strong field concentration, but also enable reaction selectivity and open pathways that are not accessible with photons by making use of hot-carrier transfer [30].

Except the resonant intramolecular excitation mechanism described above, there are other excitation mechanisms that involve charge transfer. Direct charge transfer as excitation from the metal states to the LUMO has been suggested as a possible pathway when the LSP energy is resonant with the energy gap between the metal states and LUMO, as illustrated by the arrow in Figure 1e [51].

However, many other chemical reactions are explained by the indirect hot-electron transfer mechanism, as shown by the blue arrow in Figure 1f. In this case, hot electrons are transferred from the metal to the molecule by an electron tunneling process, resulting in a transit negative ion state of the adsorbed molecule [36]. In plasmonic hot-carrier chemistry on metal surfaces, most reactions are explained by this mechanism. Besides, recent studies suggested hot-hole transfer as the reaction pathway [52]. Finally, the local heating effect, caused by the energy dissipation of the hot-carrier via the electron-phonon scattering can also induce thermal reactions of the molecules [53-55].

From the theoretical viewpoint, even though recent simulations have

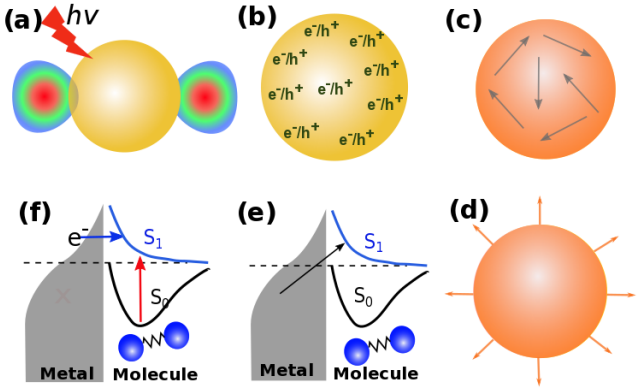


Figure 1: a) Excitation of LSP. b) Hot electron-hole pairs generation from the decay processes of the LSP. c) hot-carriers relaxation via electron-electron and electron-phonon scattering. d) Heat dissipation to the environment via thermal conduction. e-f) Excitation mechanisms of molecules adsorbed on the metal surfaces: e) direct charge transfer (black arrow), f) direct intramolecular excitation enhanced by local field of LSP (red arrow) and indirect charge transfer (blue

identified fundamental limitations when extracting hot carriers for solar energy conversion [29], the opportunities and the detailed mechanisms for using plasmonic hot-carrier extraction to drive photochemistry are less well known. Moreover, even the same chemical reactions are explained by different mechanisms [30]. Hence, understanding plasmon driven chemistry in a realistic environment from the atomistic viewpoint is crucial for further development. In our recent work [56], we demonstrated the principles of plasmonic enhancement and control of chemical reactions by considering the photoinduced dissociation of an adsorbed molecule on a plasmonic nanoparticle and plasmonic dimer.

# Atomistic study of Plasmonic Hot-Carrier Mediated Photochemical Reactions

In the following, we illustrate simulations of the plasmonic hot-carrier mediated photochemical reactions [56]. We demonstrate the principles of the plasmonic enhancement and control of chemical reactions by considering the photoinduced dissociation of an adsorbed molecule on a plasmonic nanoparticle and plasmonic dimer. The results show that the hot-carrier transfer to the antibonding orbital of $H_2$ attached to a monomer nanoparticle is quite feasible and can lead to dissociation. However, for the plasmonic dimer, a competing process involves sequential transfer of the electron to $H_2$ and then to the other nanoparticle. This reduces dissociation yield, which becomes tunable depending on the spatial location of the molecule in between the nanoparticles, with the minimal dissociation being associated with the most-significant electromagnetic hot spot.

## Computational Approach

Non-adiabatic molecular dynamics (NAMD) and Non-adiabatic excited-state molecular dynamics (NEXMD) have become powerful tools in quantum chemistry for the research of ultrafast nonadiabatic processes [57-59], thus it is ideal for the simulation of the dynamics of $H_2$ on the surface of NP following photoexcitation. Ab initio NAMD simulations are performed for $H_2$ dissociation into individual hydrogen atoms on metallic NPs after being excited by femtosecond laser pulses by employing time-dependent density functional theory (TDDFT) and Ehrenfest dynamics implemented in the OCTOPUS package [60-62], with the metal NP treated in the Jellium approximation. The Jellium radius is carefully chosen so that the resonant frequencies (around 2.5 eV) are similar to that of an Au nanoparticle with a diameter of several nanometers. For feasibility, we chose the size of the metallic NP (diameter) to be 19.05 Å, roughly corresponding to a 200 atom gold cluster. While this size is smaller compared to current experimentally relevant dimensions, the plasmonic properties of such particles are similar to those of much larger particles, except for a size-dependent blue shift of the plasmon [63]. The distance between the $H_2$ molecule and NP is set to be 1.59 Å. In addition, the $H_2$ molecule is placed parallel to the NP surface, as shown by the schematic diagram in Figure 1a. A maximum field strength of $E_{max}$ = 2.57 V/Å is assumed for the laser pulse in the simulations. The nanoparticle is approximated as Jellium medium with a single electron radius (Wigner-Seitz radius) [57] of $r_s$ = 4.5 au. The radius is carefully chosen so that the resonant frequencies of the NP are similar to that of Au nanoparticles with a diameter of several nanometers. The diameter of the NP is 38 au., which assumes 64 free electrons in the NP. The local density

approximation (LDA) is employed in the calculation. The choice of LDA functional in this work underestimates the HOMO–LUMO gap of $H_2$. However, this does not affect the physics and conclusions. Using other functionals, such as PBE, gives similar results. The grid in real space is set as 0.5 au. NAMD is treated within the Ehrenfest scheme with temperature fluctuation around room temperature (300 K). The ground state is used as the initial state for NAMD simulations. A time step of 0.1 au is used in the calculation. For the optical absorption spectrum, an electrical pulse with a strength of 0.01 au is used.

The contribution (weight) of $H_2$ to each wavefunction (WF) is estimated by integrating the WFs in a sphere centered at each H atom with a radius of 3 Å, i.e.,

$$w_i = \int_{r\leq 3\ \&\ r\notin NP} \phi_i(r)\phi_i^*(r)d\boldsymbol{r}$$

It should also be noted that the choice of radius does not affect our conclusion. If a smaller radius is used to estimate the WF weight, a similar result (LDOS of $H_2$ for different bond lengths) can also be obtained (with the only difference being that the WF weights become smaller). The charge around the $H_2$ is calculated by integrating the charge density within 3 Å of the $H_2$ molecule. According to our test, 3 Å is a reasonable threshold, which is able to characterize the $H_2$ density. A radius larger than 3 Å (recall that the position in the Jellium approximation is excluded in the integration) does not increase the charge number on $H_2$. Similarly, the charge on Au is calculated by integrating charge density within 15 Å (excluding the volume used to calculate the $H_2$ charge).

The external electric field of the light to drive the photochemical reaction is set to

$$E(t) = E_0 \exp\left[-\frac{(t-t_0)^2}{2\tau^2}\right] \cos\left[\omega(t-t_0)\right].$$

Here $\omega$ is the excitation frequency, $E_0$ is the maximum field strength of the laser pulse, $\tau = 1.6$ fs is the width of the pulse, and $t_0 = 6.6$ fs is the center of the pulse. Figure 2 indicates that a critical laser intensity is required to observe $H_2$ dissociation within 100 fs, and similar phenomena were also observed in a recent experiment [25]. In addition, it should be noted that the laser intensity used in this work is much higher than that in the experiment due to the following: (a) we need to observe the $H_2$ dissociation within tens of femtoseconds due to the limitation in computational cost; (b) even though the laser field seems very strong, the pulse duration is very short (~10 fs) compared

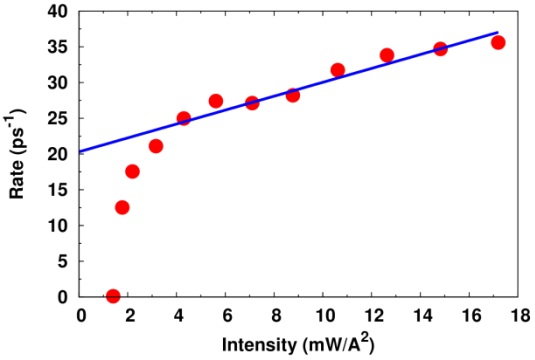


Figure 2. $H_2$ dissociation rate (defined as the inverse of time required for splitting the H-H bond when its length reaches 2.0 Å) as a function of laser intensity. According to the plot, a critical laser intensity is required to observe $H_2$ dissociation. The rate is defined as vanishing if dissociation is not observed within 100 fs. Besides, the rate is linearly dependent on the laser intensity when it is larger than 4 mW/Å$^2$. The blue line is a linear-fit of rate for laser intensity larger than 4 mW/Å$^2$.

pl

to the illumination time (~1 s) used in the experiment, and (c) the plasmon enhancement in our model is expected to be smaller than that in the experiment because the experiment involves larger particles and aggregates that have more accessible electromagnetic hot spots.

**Plasmonic Hot-Carrier-Induced $H_2$ Dissociation on the NP Surface**

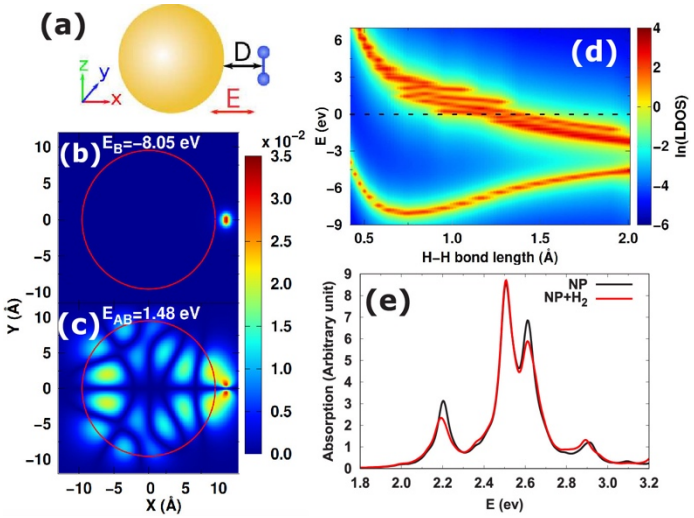


Figure 3. (a) Schematic diagram of $H_2$ molecule adsorbed on the NP surface. The electric field is in *x* direction. (b) Bonding and (c) antibonding (AB) wave functions of $H_2$ in the *x*–*z* plane. Panel c indicates that (1) the AB state is 1.48 eV above the Fermi energy, which offers the possibility of transferring the hot-electron generated in the metallic NPs to the AB state; and (2) the AB WF is hybridized with the NP, which can facilitate the hot-electron transfer. The red circle indicates the surface of the NP. (d) LDOS of $H_2$ adsorbed on NP surface. The dashed line indicates the Fermi energy (shifted to 0) of the NP + $H_2$ system with equilibrium H–H bond length. The evolution of peaks in LDOS for different H–H bond lengths roughly reflects the PES of the $H_2$molecule. (e) Absorption spectrum of NP and NP-$H_2$.

We start by examining the electronic structure of $H_2$ adsorbed on the NP, where the wave functions (WFs) of $H_2$ and the NP become hybridized at chemically relevant separations. Analysis of the weight (wi) of $H_2$ to each WF shows that the bonding and antibonding (AB) state (the states that have the largest wi) of the $H_2$ are 8.05 eV below and 1.48 eV above the Fermi energy, respectively, as shown by Figure 3b–d. Because the 9.53 eV gap between the bonding and AB states of $H_2$ is much larger than the energy of a visible light quantum, no electron in the bonding state of $H_2$ can be excited by a photon to the AB state to drive the chemical reaction in the visible regime. However, in the

coupled system, the AB state is only 1.48 eV above the Fermi level, which suggests the possibility of transferring hot electrons generated in the metallic NP to the AB state of $H_2$ and inducing chemical reaction such as $H_2$ dissociation. In addition, Figure 3b also shows that the AB WF of $H_2$ is strongly hybridized with the NP, which can also facilitate interfacial hot-electron transfer by directly exciting an electron of the NP to the attached molecule, as demonstrated in recent experiments [51, 64−65]. Because the excitation of electron–hole pairs by plasmon decay in the NP can generate hot electrons with energy ranging from zero to the photon energy (which, in this example, means that the energy of the hot-electron can be larger than 1.48 eV) [29,66,67], our results suggest that $H_2$ dissociation can be readily induced by the hot electrons generated in the metallic NP. In addition, the local density of states (LDOS) of $H_2$ for different H–H bond lengths is plotted in Figure 3d. The evolution of peaks in LDOS for different H–H bond lengths roughly reflects the potential energy surface (PES) of the $H_2$. The plot shows the evolution of bonding and AB states of $H_2$ with varying bond lengths. Even though the $H_2$ molecule is coupled to the NP and the WFs are hybridized, the PES of $H_2$ is similar to that of the standalone $H_2$ molecule. NAMD for the standalone $H_2$ molecule also confirms that dissociation can indeed occur upon promoting electrons to the antibonding state. Hence, the PES shown in the plot reveals that when the $H_2$ is attached to the NP, electron transfer from the NP to the AB state of $H_2$ is feasible and is able to drive $H_2$ dissociation by following the molecular dynamics on the excited state PES.

The absorption spectra of NP and NP-$H_2$ are shown in Figure 3e. The spectrum of the NP shows four resonant absorption peaks that are all plasmonic, as confirmed by the TDDFT calculation, in which collective excitations are observed. These four peaks correspond to different plasmon modes [68]. Here we note that interband effects are not included in the Jellium model, so the optical properties of Au in this model are more plasmonic than they would be in a more-realistic description of Au. The distribution of the induced charge and field enhancement for each mode can be found in Figure 3a,b. When $H_2$ is absorbed on the NP surface, the absorption spectrum is weakly perturbed essentially through slightly larger broadening (i.e., damping) of the peaks. This observation is attributed to the WF hybridization between the $H_2$ and the NP, which alters the electronic structure, as well as to the collective electron oscillation (plasmon) to some extent. However, the four resonant peaks remain virtually unchanged. The absorption spectrum in the visible is dominated by the NP even though the AB state of $H_2$ is hybridized with the NP. Because the NP shows stronger absorption and field enhancement at the resonant frequencies, we next study the dynamics of these states. Namely, four resonant energies ($\omega$ = 2.23, 2.53, 2.63, and 2.93 eV) of the NP are used to excite the NP and to

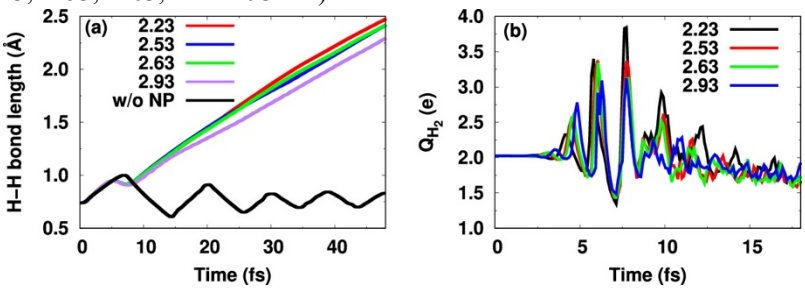


Figure 4. (a) Real-time dynamics of $H_2$ bond length with and without NP. For the case of $H_2$ alone, the excitation frequency is 2.53 eV. By coupling to the NP, plasmonic hot-carrier mediated induced chemical reaction is observed. (b) Time evolution of charge around $H_2$ after photoexcitation with different frequencies.

calculate the subsequent plasmonic hot-carrier-mediated chemical reactions.

Figure 4a plots the time evolution of the H–H bond length (with and without NP) excited by the external field with different excitation energies. The black curve shows that the $H_2$ bond oscillates with the external field and never dissociates if the $H_2$ is not coupled to the NP. Because the energy of incident light is much smaller than the HOMO–LUMO gap, an external field can only perturb the charge density and drive the hydrogen molecule to vibrate near the equilibrium position. However, if the $H_2$ is placed near the NP surface, plasmon excitation at any resonant energy results in an increase in the $H_2$ bond length. The H–H bond reaches 2 Å in less than 40 fs, indicating molecular dissociation. Because the Jellium model with no explicit Au atoms is used in our work, the Au–H interaction is not correctly captured, i.e., the adsorption and desorption behavior of H atoms on the NP surface is poorly described compared to the atomistic model of NP [69]. Consequently, lacking bonding to Au, the H atoms drift away after dissociation. In realistic experiments, there are several $H_2$ molecules making it more probable for the dissociated protons/H atoms to meet and recombine into molecular hydrogen. Actually, the experiment on $H_2$ dissociation (mixed with $D_2$) by Halas group detected the generation of HD to estimate the reaction rate [34].

To illustrate the charge-transfer behavior, we also analyze the charge dynamics upon laser excitation. Figure 4b shows the charge around $H_2$, which is calculated by integrating the charge density within 3 Å of the $H_2$ molecule. Following the oscillations of the external field, the $H_2$ charge also oscillates with time, which indicates forward and backward charge transfer between the NP and $H_2$ molecule. Initially, the charge on $H_2$, $Q_{H2}$, is around 2 e (elemental charge). After photoexcitation, the charge of $H_2$ increases to 3.1–3.8 e at around 7.7 fs. The additional charge transferred from the NP resides on the AB states of $H_2$, thus initiating motion along the excited potential energy surface and dissociating the molecule. Figure 4b shows that the amount of charge transferred to $H_2$ varies for different excitation energies. Consequently, different excitation energies can result in slightly different dissociation rates because the distribution of induced charge density and field enhancement for different plasmon modes are different as shown in Figure 5a,b. If the excitation energy tunes away from the plasmon resonant energies, the field-enhancement and induced charges become smaller. Consequently, the dissociation rates are reduced. In addition, the charge transfer is also dependent on light intensity. Generally, increasing the light intensity increases the amount of charge transferred to $H_2$ because the intensity of hot-carriers generated from the plasmon decay is proportional to light intensity in the linear response regime.

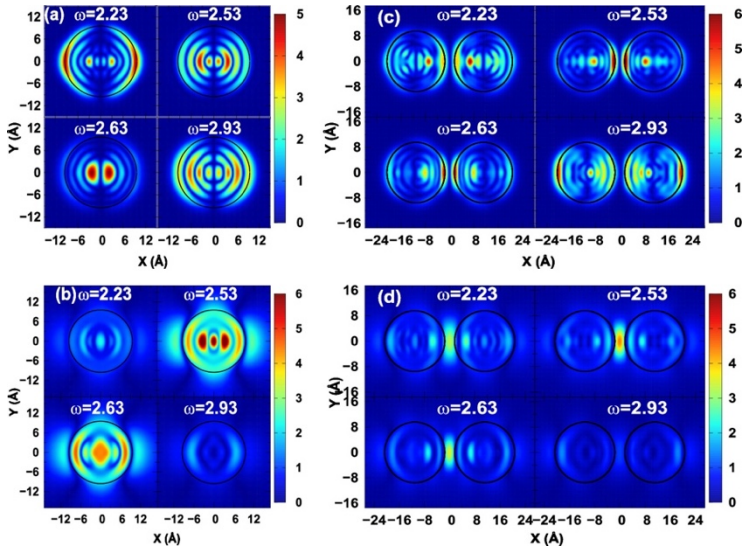


Figure 5. Induced charge (in unit of $10^{-4}$ e) distribution for (a) single NP and (c) NP dimer (d = 1.59 Å); Profile of field-enhancement $\left(\left|\frac{E_{incident}(\omega)}{E_{incident}(\omega)}\right|\right)$ for (b) single NP and (d) NP dimer. The single NP enhances the field at both ends of the NP in the direction of the external field. The NP dimer can generate hot-spots in the gap, and the field enhancement in the dimer gap is also found to be larger than that near the surface of the single NP (except for 2.93 eV).

## Tunable $H_2$ Dissociation in the Plasmonic Dimer

In practical applications, an assembly of NPs instead of a single NP is usually employed, allowing for the formation of dimers and other aggregates that have more significant electromagnetic hot spots and charge-transfer plasmons [70]. Indeed, plasmonic NP aggregates and arrays have many novel optical properties and have found promising applications in various fields, including lasing, sensing, and quantum information processing [71]. As shown in Figure 5, the distribution of induced charge and field enhancement in the plasmonic dimer is very different from that of a NP monomer. In contrast to a single NP, the field enhancement of the plasmonic dimer is spatially located in the gap between the two NPs and is more significant than that in the near-field of a NP monomer. Because photodissociation also depends on light intensity, as evidenced by Figure 2, the stronger field in the spatial gap presumably may further promote dissociation. Moreover, as we discussed above, the stronger field intensity is also able to induce more hot electrons, an effect confirmed

theoretically and experimentally [72,73]. Thus, it is natural to consider if the stronger field enhancement in NP aggregates can facilitate $H_2$ dissociation. Consequently, we calculated $H_2$ dissociation in the plasmonic dimer for different geometrical configurations.

As an example of the photochemistry for the dimer structure, we consider

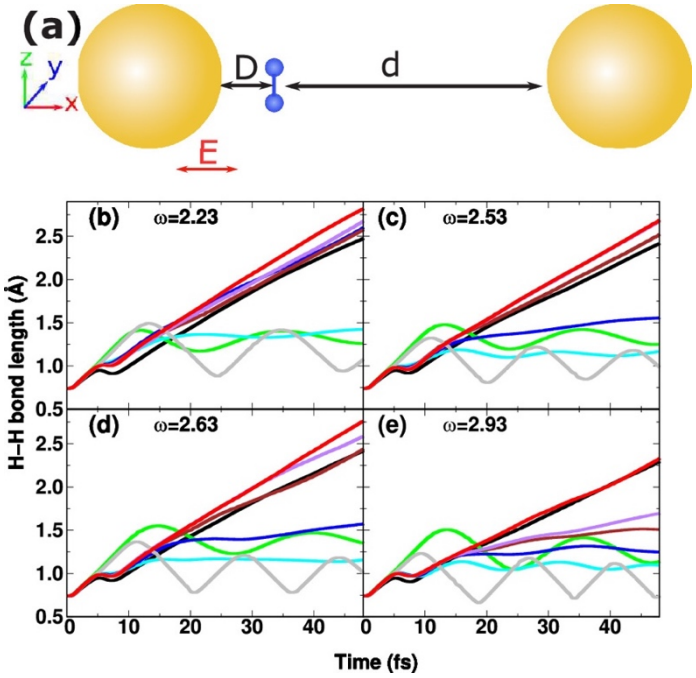


Figure 6. Bond dynamics of $H_2$ in plasmonic dimer with different distance. $H_2$ dissociation in a dimer of a pair of 1.9 nm NPs with different distances (for D = 1.59 Å): monomer (black), d = 1.59 Å (green), d = 3.70 Å (cyan), d = 5.82 Å (blue), d = 7.94 Å (brown), d = 10.05 Å (purple), d = 12.17 Å (red), and D = d = 5.82 Å (gray). Photochemical reaction for d = 1.59 Å is significantly suppressed. Tuning the distance d can affect the dynamics of $H_2$ in the plasmonic dimer.

the $H_2$ molecule placed between the NPs. The distance between $H_2$ and one of the NPs is fixed at 1.59 Å (which we define as the distance D), which is the same as in the case studied above. The distance between $H_2$ and the other NP is d, taken as a variable. A schematic diagram of the configuration is shown in Figure 6a. The time evolution of H–H bond lengths for different d is plotted in Figure 6b–e. When d = D = 1.59 Å, the $H_2$ is placed precisely in the center of the plasmonic dimer, with the stronger field enhancement compared to larger values of d. It should be noted that there is a critical distance between the two NPs at which the field-enhancement is strongest for a general plasmonic dimer [74]. In our case, the smallest separation between the two NPs is 3.18 Å for d =

D, and the field enhancement decreases monotonically with increasing d. In this configuration, the induced charges (hot electrons) are enhanced in the gap edges (Figure 5c) except for 2.93 eV. The latter is an example of plasmonic resonance in which the induced charges are not magnified at the gap edges. However, no matter what the excitation energy is, the H–H bond never breaks, as shown by the green curves in Figure 6. Even though Figure 6 suggests that, for geometries with smaller d, the H–H bond length can significantly increas to 1.2–1.4 Å, which is larger than the equilibrium value, the dissociation event does not occur, as evidence by the subsequent oscillatory dynamics of the bond length.

Our NAMD simulations further demonstrate that tuning the distance d can affect the dynamics significantly. As shown in Figure 6, the $H_2$ starts to dissociate for some excitation frequencies when d reaches 5.82 Å. It should be noted that d = 5.82 Å may be not a precise critical distance that separates the two phases ($H_2$ dissociation or lack of dissociation) because we did not sample the distance d with sufficiently small increments due to the computational cost. However, for a given light intensity and photon energy, a critical distance that separates the two phases exists. This critical distance can vary with excitation energy (or plasmon mode) because different plasmon modes induce different charge distributions, field enhancements, and dissociation rates, as shown in Figures 4a,b, and 5a. For instance, for the mode at 2.93 eV, which has a smaller dissociation rate as shown in Figure 4a, larger d is required to restore the chemical reaction, as seen in Figure 6e. To illustrate the importance of the relative position of the $H_2$ molecule in the plasmonic dimer, we studied the $H_2$ dynamics in the NP dimer with D = d = 5.82 Å. Here, the distance between the two NPs is 11.64 Å, which corresponds to the arrangement with D = 1.59 Å and d = 10.05 Å. As shown by the gray line in Figure 6, no dissociation is observed in this case, which, however, is similar to the outcome with geometry D = d = 1.59 Å. The difference is that when D = d = 5.82 Å, the bond-fluctuation time scale becomes faster. Moreover, the distance between the $H_2$ and the NP (5.82 Å) is much larger than 1.59 Å, so the coupling between the $H_2$ and the NP is much smaller compared to that for the D = d = 1.59 Å geometry, and the $H_2$ dynamics are closer to those of the pure $H_2$ case, as shown by the black curve of Figure 4a. An even-larger distance d more strongly favors dissociation of the H–H bond. These results demonstrate that chemical reaction can either be suppressed or enhanced by the plasmonic dimer depending on the relative position of the molecule between the dimer. Thus, hot-carrier-mediated dissociation can be tuned by controlling the location of the molecule in the spatial gap. For the NP dimer, the optical properties are also different from that of a single NP, especially for small d. According to our calculation, compared to a single NP, the resonant peaks are shifted in a dimer with the shift increasing with decreasing d. Some peaks are blue-shifted, and the others are red-shifted because coupling ($\Delta$) between the two NPs can split a resonant energy ($\omega$) into satellite $\omega \pm \Delta$ components. This suggests modeling the $H_2$ dynamics in the NP

dimer for d = 1.59 Å with the new resonant energies. However, the results (not shown) also indicate the absence of $H_2$ dissociation, even when the $H_2$ is excited at the resonant energies of the NP dimer.

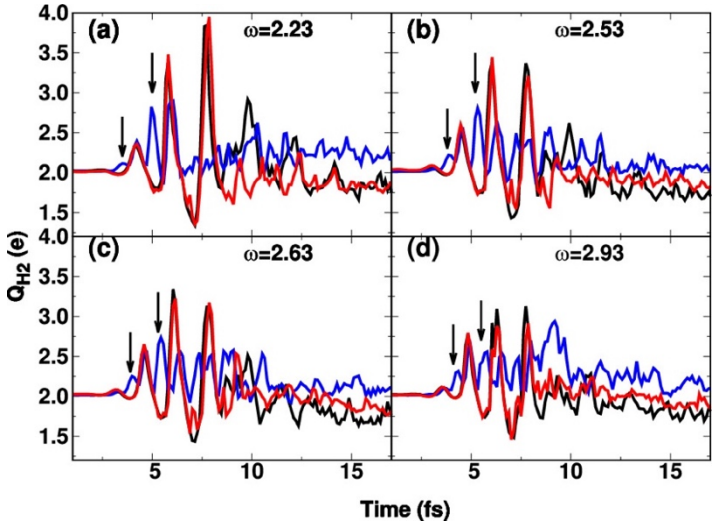


Figure 7. Charge of $H_2$ on the surface of single NP (black) and in plasmonic dimer with different d: d = 1.59 Å (blue) and d = 12.17 Å (red). In general, the larger distance increases the charge accumulation on the $H_2$ molecule. For d = 1.59 Å, the hot electrons transferred from the left NP quickly transfer to the right NP, which reduces the net charge accumulation on $H_2$. Thus, the photochemical reaction is getting suppressed.

We have further examined the charge dynamics of the $H_2$ molecule in the NP dimer gap when excited by different photon energies. The results are plotted in Figure 7, and the charge difference between the two nanoparticles as well as the charges of each NP are plotted in Figure 8. When d = 1.59 Å, the charge dynamics on the $H_2$ molecule shows high-frequency oscillations (enhanced by a factor of 2) but with reduced amplitudes compared to $H_2$ on the surface of the NP monomer. In addition, Figure 8 shows that the charge oscillates back and forth between the two NPs with a frequency that is comparable to that seen for the NP monomer. These two figures show that when the NPs are close together and the $H_2$ molecule is midway between them, the charge evolves coherently from one particle to the molecule and to the other particle and then back, with the doubled frequency at the position of the molecule reflecting a small difference in phasing of the charge flow to the molecule and then from the molecule to the receiving particle. We also note that the charge amplitude changes from −4 to +4 for the particles in Figure 8, while the corresponding change on the $H_2$ is less than 0.5 in magnitude. Hence, compared to the single-NP case (the black curve in Figure 7), the charge accumulation on $H_2$ is reduced

in presence of the NP dimer, which makes the dissociation much less probable. When d = 12.17 Å, the charge oscillation becomes the same as in the single NP case, which indicates that this value of d is sufficient to suppress the second consequent charge transfer. The maximum charge on $H_2$ can reach as high as 3.8 e in this case, which significantly increases the dissociation probability.

Overall, we see that hot carriers transferred from one NP to the $H_2$ will undergo another charge transfer to the other NP before $H_2$ dissociation can develop when d = 1.59 Å. Increasing the distance d makes the charge-transfer rates different. Indeed, in the red curves in Figure 7, we see that the time scale of charge oscillation is the same as for the single-NP case. With increasing distance, the charge loss from the $H_2$ molecule to the right NP is suppressed. At a certain distance, the charge accumulation on $H_2$ can be large enough to induce bond dissociation. This is the reason why a critical distance exists for inducing $H_2$ dissociation in the plasmonic dimer. Because the right NP still has a significant contribution to the field enhancement in the gap for d = 12.17 Å, dissociation can be enhanced relative to the monomer case for certain d values and plasmon modes.

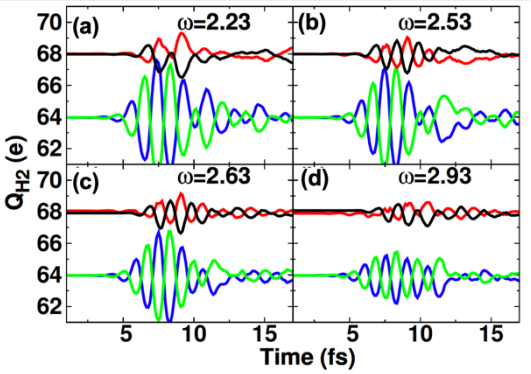


Figure 8. (a-d) Time evolution of charges on NPs for d = 0 (blue for the left NP, green for the right NP) and d = 12.17 Å (red for the left NP, black for the right NP). The charges for the d = 12.17 Å are shifted by 4 e for clarity. The evolution of charges on the two NPs indicates there is significant charge transfer for the case of d = 1.59 Å .

## Discussions

In realistic applications, the $H_2$ molecules would typically have a broad spatial distribution of possible locations on the dimer. Such placement would be difficult to control with any precision. Hence, only a fraction of the $H_2$ molecules in a strong plasmonic field can be dissociated by exciting plasmonic

hot carriers. To improve efficiency, charge transfer from the $H_2$ molecule to one of the NPs needs to be suppressed. One approach is to coat one of the particles with $SiO_2$. Recent experiments have indicated that the large barrier between $SiO_2$ and a metallic NP can practically eliminate hot electron transfer [75]. In addition, it should be noted that plasmon-driven hot-electron transfer to adsorbed molecules (in this case, the molecule 4,4′-bipyridine, BPY that has a stable negative ion) has been confirmed in a recent experiment using SERS techniques [77]. This study also found that the negative ion has a finite lifetime, indicating that additional charge-transfer processes occur after the negative ion is formed. Unfortunately, the time scale of charge-transfer processes in that work were only studied at time scales greater than 1 s.

Finally, we note that the mechanism of suppression of chemical reaction in the plasmonic dimer proposed in our work is fundamentally different from that studied in [77], where the quantum nature of the cavity plays a vital role in modifying the PES of the molecule [78,79]. In contrast, in our case, the balance between charge transfer and field enhancement tunes the chemical reaction, and strong coupling leading to the formation of a new polaritonic state is not needed. Another aspect of the difference in the mechanisms is that the suppression of chemical reaction when d = 1.59 Å holds for different excitation frequencies, including nonresonant regime. The mechanism in [77] is only observed for resonant excitation because hybridization between the electronic and photonic states becomes important only when the excitation energy is resonant with the cavity [78].

## Summary and Outlook

In summary, we have introduced a different mechanism potentially leading to plasmon-enhanced photochemistry. Performed TDDFT and NAMD calculations allow monitoring the dynamic process of $H_2$ dissociation on the surface of a metallic NP mediated by hot-carrier transfer. Our results illustrate the phenomenon of plasmon-induced $H_2$ dissociation at the atomic scale and identify how hot carriers can be transferred from a NP to the adsorbed molecule to drive photochemistry. The electronic structure calculations show significant wave function hybridization between NP and $H_2$ and that the energy difference between the AB state and the Fermi level makes dissociation accessible by the visible light. In addition, because photoinduced charge transfer can be controlled by the shape of the external field, we can imagine adjusting laser parameters and nanoparticle size to control electronic hybridization and dynamics to direct the plasmon-assisted photochemistry.

Our results also demonstrate that the photochemistry can be tunable in the case of a plasmonic dimer. When the molecule is placed in the center of NP dimer, charge transfer between the molecule and each of the two NPs is

identical. Consequently, the hot electrons transferred to the molecule from one of the NP are transferred to the other nanoparticle before the dissociation can occur. As a result, the effective charge accumulation on the molecule is reduced, and the chemical reaction is suppressed. By tuning the relative position of the molecule in the spatial gap of the NP dimer, one of these charge-transfer processes can be efficiently suppressed. Consequently, charge accumulation on the molecule can be enhanced and the chemical reactions thus restored. This indicates that via geometry control, field enhancement can be increased and charge loss minimized. Even though our conclusions are based on $H_2$ dissociation, the concept can be applied to other cases, such as water splitting [80-82]. In practical applications, the loss of charge from an adsorbate to the NP can be suppressed via coating of the latter by insulating materials, such as $SiO_2$.

In addition, different mechanisms have been proposed to explain the plasmon-mediated chemical reactions of different molecules. Even the same chemical reaction have been explained by different mechanisms [30]. In order to investigate and distinguish the mechanisms of plasmon-induced chemical reactions, experimental techniques with high spatial/time resolution and advanced electronic structure calculations are required. Via combination of experimental and theoretical efforts, detailed understanding of the different pathways involved in plasmon mediated chemical reactions is expected to be achieved [30].

## Acknowledgement

The work at Los Alamos National Laboratory (LANL) was supported by the LANL Directed Research and Development Funds (LDRD) and performed in part at the Center for Integrated Nanotechnologies (CINT), a U.S. Department of Energy, Office of Science user facility at LANL. This research used resources provided by the LANL Institutional Computing (IC) Program. LANL is operated by Triad National Security, LLC, for the National Nuclear Security Administra- tion of the U.S. Department of Energy (Contract No. 89233218NCA000001).

## Reference

[1] Tame, M. S.; McEnery, K. R.; Ozdemir, S. K.; Lee, J.; Maier, S. A.; Kim, M. S. Quantum Plasmonics. *Nat. Phys*. **2013**, 9, 329–340.

[2] Archambault, A.; Marquier, F.; Greffet, J.-J.; Arnold, C. Quantum Theory of Spontaneous and Stimulated Emission of Surface Plasmons. *Phys. Rev. B* **2010,** 82, 035411.

[3] Ballester, D.; Tame, M. S.; Lee, C.; Lee, J.; Kim, M. S. Long-Range Surface-Plasmon-Polariton Excitation at The Quantum Level. *Phys. Rev. A* **2009**, 79, 053845.

[4] Kottmann, J. P.; Martin, O. J. F.; Smith, D. R.; Schultz, S. Plasmon Resonances of Silver Nanowires with a Nonregular Cross Section. *Phys. Rev. B* **2001**, 64, 235402.

[5] Kelly, K. L.; Coronado, E.; Zhao, L. L.; Schatz, G. C. The Optical Properties of Metal Nanoparticles: The Influence of Size, Shape, and Dielectric Environment. *J. Phys. Chem. B* **2003**, 107, 668–677.

[6] Moskovits, M. Surface-Enhanced Spectroscopy. *Rev. Mod. Phys.* **1985**, 57, 783.

[7] Stiles, P. L.; Dieringer, J. A.; Shah, N. C; Van Duyne, R. P. urface-Enhanced Raman Spectroscopy. *Annu. Rev. Anal. Chem.* **2008**, 601-626.

[8] Gersten, J. I.; Nitzan, A. Photophysics and photochemistry near surfaces and small particles. *Surf. Sci.* **1985**, 158, 165-189.

[9] Anger, P.; Bharadwaj, P.; Novotny, L. Enhancement and Quenching of Single-Molecule Fluorescence. *Phys. Rev. Lett.* **2006**, 96, 113002.

[10] Atwater, H. A.; Polman, A. Plasmonics for Improved Photovoltaic Devices. *Nat. Mater.* **2010**, 9, 205-213.

[11] Kazuma, E.; Jung, J.; Ueba, H.; Trenary, M.; Kim, Y. Real-Space and Real-Time Observation of a Plasmon-Induced Chemical Reaction of a Single Molecule. *Science* **2018**, 360, 521-526.

[12] Brongersma, M. L.; Halas, N. J.; Nordlander, P. Plasmon-Induced Hot Carrier Science and Technology. *Nat. Nano*. **2015**, 10, 25–34.

[13] Li, X.; Xiao, D.; Zhang, Z. Landau Damping of Quantum Plasmons in Metal Nanostructures. *New J. Phys*. **2013**, 023011.

[14] Frischkorn, C.; Wolf, M. Femtochemistry at Metal Surfaces: Nonadiabatic Reaction Dynamics. *Chem. Rev.* **2016**, 4207-4233.

[15] West, P.; Ishii, S.; Naik, G.; Emani, N.; Shalaev, V.; Boltasseva, A. Searching for Better Plasmonic Materials. *Laser Photonics Rev.* **2010**, 4, 795–808.

[16] Tisdale, W. A.; Williams, K. J.; Timp, B. A.; Norris, D. J.; Aydil, E. S.; Zhu, X.-Y. Hot-Electron Transfer from Semiconductor Nanocrystals. *Science* **2010**, 328, 1543–1547.

[17] Wang, F.; Melosh, N. A. Plasmonic Energy Collection through Hot Carrier Extraction. *Nano Lett.* **2011**, 11, 5426–5430.

[18] Clavero, C. Plasmon-Induced Hot-Electron Generation at Nanoparticle/Metal-Oxide Interfaces for Photovoltaic and Photocatalytic Devices. *Nat. Photon*. **2014**, 8, 95–103.

[19] Dong, Y.; Choi, J.; Jeong, H.-K.; Son, D. H. Hot Electrons Generated from Doped Quantum Dots via Upconversion of Excitons to Hot Charge Carriers for Enhanced Photocatalysis. J. Am. Chem. Soc. 2015, 137, 5549–5554.

[20] Baffou, G.; Quidant, R. Nanoplasmonics for Chemistry. Chem. Soc. Rev. 2014, 43, 3898–3907.

[21] Boriskina, S. V.; Ghasemi, H.; Chen, G. Plasmonic Materials for Energy: From Physics to Applications. Mater. Today 2013, 16, 375 – 386.

[22] Fang, Z.; Wang, Y.; Liu, Z.; Schlather, A.; Ajayan, P. M.; Koppens, F. H. L.; Nordlander, P.; Halas, N. J. Plasmon-Induced Doping of Graphene. ACS Nano 2012, 6, 10222–10228.

[23] Hong, T.; Chamlagain, B.; Hu, S.; Weiss, S. M.; Zhou, Z.; Xu, Y.-Q. Plasmonic Hot Electron Induced Photocurrent Response at MoS2-Metal Junctions. ACS Nano 2015, 9, 5357–5363.

[24] Reineck, P.; Brick, D.; Mulvaney, P.; Bach, U. Plasmonic Hot Electron Solar Cells: The Effect of Nanoparticle Size on Quantum Efficiency. J. Phys. Chem. Lett. 2016, 7, 4137–4141.

[25] Knight, M. W.; Sobhani, H.; Nordlander, P.; Halas, N. J. Photodetection with Active Optical Antennas. Science 2011, 332, 702–704.

[26] Zhang, Y.; He, S.; Guo, W.; Hu, Y.; Huang, J.; Mulcahy, J. R.; Wei, W. D. Surface-Plasmon-Driven Hot Electron Photochemistry. Chem. Rev. 2017, 118, 2927–2954.

[27] Naik, G. V.; Dionne, J. A. Photon Upconversion with Hot Carriers in Plasmonic Systems. Appl. Phys. Lett 2015, 107, 133902.

[28] Kojori, H. S.; Yun, J.-H.; Paik, Y.; Kim, J.; Anderson, W. A.; Kim, S. J. Plasmon Field Effect Transistor for Plasmon to Electric Conversion and Amplification. Nano Lett. 2016, 16, 250–254.

[29] Zhang, Y.; Yam, C.; Schatz, G. C. Fundamental Limitations to Plasmonic Hot-Carrier Solar Cells. J. Phys. Chem. Lett. 2016, 7, 1852–1858.

[30] Kazuma, E.; Kim, Y. Mechanistic Studies of Plasmon Chemistry on Metal Catalysts. *Angew. Chem. Int. Ed.* **2019**, 58, 2-11.

[31] Palczewski, K. Chemistry and Biology of Vision. J. Bio. Chem. 2012, 287, 1612–1619.

[32] Blankenship, R. Molecular Mechanisms of Photosynthesis; John Wiley & Sons, 2014.

[33] Zemelman, B. V.; Nesnas, N.; Lee, G. A.; Miesenböck, G. Photochemical Gating of Heterologous Ion Channels: Remote Control over Genetically Designated Populations of Neurons. Proc. Nat. Acad. Sci. 2003, 100, 1352–1357.

[34] Mukherjee, S.; Libisch, F.; Large, N.; Neumann, O.; Brown, L. V.; Cheng, J.; Lassiter, J. B.; Carter, E. A.; Nordlander, P.; Halas, N. J. Hot Electrons Do the Impossible: Plasmon-Induced Dissociation of H2 on Au. Nano Lett. 2013, 13, 240–247.

[35] Libisch, F.; Cheng, J.; Carter, E. A. Electron-Transfer-Induced Dissociation of H2 on Gold Nanoparticles: Excited-State Potential Energy Surfaces via Embedded Correlated Wavefunction Theory. Z. Phys. Chem. 2013, 227, 1455–1466.

[36] Linic, S.; Aslam, U.; Boerigter, C.; Morabito, M. Photochemical Transformations on Plasmonic Metal Nanoparticles. Nat. Mater. 2015, 14, 567-576.

[37] Christopher, P.; Xin, H.; Marimuthu, A.; Linic, S. Singular Characteristics and Unique Chemical Bond ActivationMechanisms of Photocatalytic Reactions on Plasmonic Nanostructures. Nat. Mater. 2012, 11, 1044.

[38] Mukherjee, S.; Zhou, L.; Goodman, A. M.; Large, N.; Ayala-Orozco, C.; Zhang, Y.; Nordlander, P.; Halas, N. J. Hot-Electron-Induced Dissociation of H2 on Gold Nanoparticles Supported on SiO2. J. Am. Chem. Soc. 2014, 136, 64–67.

[39] Zhang, C.; Zhao, H.; Zhou, L.; Schlather, A. E.; Dong, L.; McClain, M. J.; Swearer, D. F.; Nordlander, P.; Halas, N. J. Al-Pd Nanodisk Heterodimers as Antenna-Reactor Photocatalysts. Nano Lett. 2016, 16, 6677–6682.

[40] Swearer, D. F.; Zhao, H.; Zhou, L.; Zhang, C.; Robatjazi, H.; Martirez, J. M. P.; Krauter, C. M.; Yazdi, S.; McClain, M. J.; Ringe, E.; Carter, E. A.; Nordlander, P.; Halas, N. J. Heterometallic Antenna-Reactor Complexes for Photocatalysis. Proc. Nat. Acad. Sci. 2016, 113, 8916–8920.

[41] Yan, L.; Ding, Z.; Song, P.; Wang, F.; Meng, S. Plasmon-Induced Dynamics of H2 Splitting on a Silver Atomic Chain. Appl. Phys. Lett. 2015, 107, 083102.

[42] Tanaka, A.; Sakaguchi, S.; Hashimoto, K. Kominami, H. Preparation of $Au/TiO_2$ with Metal Cocatalysts Exhibiting Strong Surface Plasmon Resonance Effective for Photoinduced Hydrogen Formation under Irradiation of Visible Light. *ACS. Catal.* **2013**, 3, 79-85.

[43] Zhang, Z.; Huang, J.; Fang, Y.; Zhang, M.; Liu, K.; Dong, B. A Nonmetal Plasmonic Z-Scheme Photocatalyst with UV- to NIR-Driven Photocatalytic Protons Reduction. *Adv. Mater.* **2017**, 29, 1606688.

[44] Ingram, D. B.; Linic, S. Water Splitting on Composite Plasmonic-Metal/Semiconductor Photoelectrodes: Evidence for Selective Plasmon-Induced Formation of Charge Carriers near the Semiconductor Surface. J. Am. Chem. Soc. 2011, 133, 5202–5205.

[45] Ghobadi, T. G. U.; Ghobadi, A.; Ozbay, E.; Karadas, F. Strategies for Plasmonic Hot-Electron-Driven Photoelectrochemical Water Splitting. ChemPhotoChem 2, 161–182.

[46] Naldoni, A.; Guler, U.; Wang, Z.; Marelli, M.; Malara, F.; Meng, X.; Besteiro, L. V.; Govorov, A. O.; Kildishev, A. V.; Boltasseva, A.; Shalaev, V. M. Broadband Hot-Electron Collection for Solar Water Splitting with Plasmonic Titanium Nitride. Adv. Opt. Mater. 2017, 5, 1601031.

[47] Lee, J.; Mubeen, S.; Ji, X.; Stucky, G. D.; Moskovits, M. Plasmonic Photoanodes for Solar Water Splitting with Visible Light. Nano Lett. 2012, 12, 5014–5019.

[48] Robatjazi, H.; Bahauddin, S. M.; Doiron, C.; Thomann, I. Direct Plasmon-Driven Photoelectrocatalysis. Nano Lett. 2015, 15, 6155–6161.

[49] Mubeen, S.; Lee, J.; Singh, N.; Kramer, S.; Stucky, G. D.; Moskovits, M. An Autonomous Photosynthetic Device inWhich All Charge Carriers Derive From Surface Plasmons. Nat. Nano. 2013, 8, 247–251.

[50] Hou, W.; Hung, W. H.; Pavaskar, P.; Goeppert, A.; Aykol, M.; Cronin, S. B. Photocatalytic Conversion of CO2 to Hydrocarbon Fuels via Plasmon-Enhanced Absorption and Metallic Interband Transitions. *ACS Catal*. **2011**, 1, 929–936.

[51] Boerigter, C.; Aslam, U.; Linic, S. Mechanism of Charge Transfer from Plasmonic Nanostructures to Chemically Attached Materials. ACS Nano 2016, 10, 6108–6115.

[52] Schlather, A. E.; Manjavacas, A.; Lauchner, A.; Marangoni, V. S.; DeSantis, C. J.; Nordlander, P.; Halas, N. J. Hot Hole Photochemistry on Au@SiO2@Au Nanoparticles, *J. Phys. Chem. Lett*, **2018**, 8, 2060-2067.

[53] Yu, Y.; Sundaresan, V.; Willets K. A.; Hot Carriers versus Thermal Effects: Resolving the Enhancement Mechanisms for Plasmon-Mediated Photoelectrochemical Reactions. *J. Phys. Chem. C* **2018**, 122, 5040-5048.

[54] Golubev, A. A.; Khlebtsov, B. N.; Rodriguez, R. D.; Chen, Y.; Zahn, D. R. T. Plasmonic Heating Plays a Dominant Role in the Plasmon-Induced

Photocatalytic Reduction of 4-Nitrobenzenethiol. *J. Phys. Chem. C.* **2018**, 122, 5657-5663.

[55] Bora, T.; Zoepfl, D.; Dutta, J. Importance of Plasmonic Heating on Visible Light Driven Photocatalysis of Gold Nanoparticle Decorated Zinc Oxide Nanorods. *Sci. Rep.* **2016** 6, 26913.

[56] Zhang, Y.; Nelson, T.; Tretiak, S.; Guo, H.; Schatz. G.C. Plasmonic Hot-Carrier-Mediated Tunable Photochemical Reactions. *ACS Nano*, 2**018**, 12, 8415–8422.

[57] Crespo-Otero, R.; Barbatti, M. Recent Advances and Perspectives on Nonadiabatic Mixed Quantum–Classical Dynamics. *Chem. Rev.* **2018**, 118, 7026-7068.

[58] Nelson, T.; Fernandez-Alberti, S.; Roitberg, A. E.; Tretiak, S. Nonadiabatic Excited-State Molecular Dynamics: Modeling Photophysics in Organic Conjugated Materials. *Acc. Chem. Res.* **2014**, 47, 1155-1164.

[59] Sifain, A. E.; Bjogaard, J. A.; Nelson, T. R.; Nebgen, B. T.; White, A. J.; Gifford, B. J.; Gao, D. W.; Prezhdo, O. V.; Fernandez-Alberti, S.; Roitberg, A. E.; Tretiak, S. Photoexcited Nonadiabatic Dynamics of Solvated Push–Pull π-Conjugated Oligomers with the NEXMD Software. *J. Chem. Theory Comput.* **2018**, 14, 3955-3966.

[60] Castro, A.; Appel, H.; Oliveira, M.; Rozzi, C. A.; Andrade, X.; Lorenzen, F.; Marques, M. A. L.; Gross, E. K. U.; Rubio, A. Octopus: a Tool for the Application of Time-Dependent Density Functional Theory. Phys. Stat. Sol. B 2017, 243, 2465–2488.

[61] Andrade, X.; Alberdi-Rodriguez, J.; Strubbe, D. A.; Oliveira, M. J. T.; Nogueira, F.; Castro, A.; Muguerza, J.; Arruabarrena, A.; Louie, S. G.; Aspuru-Guzik, A.; Rubio, A.; Marques, M. A. L. Time-Dependent Density-Functional Theory in Massively Parallel Computer Architectures: the Octopus Project. J. Phys. Cond. Mat. 2012, 24, 233202.

[62] Andrade, X.; Strubbe, D.; De Giovannini, U.; Larsen, A. H.; Oliveira, M. J. T.; Alberdi-Rodriguez, J.; Varas, A.; Theophilou, I.; Helbig, N.; Verstraete, M. J.; Stella, L.; Nogueira, F.; Aspuru-Guzik, A.; Castro, A.; Marques, M. A. L.; Rubio, A. Real-Space Grids and the Octopus Code as Tools for the Development of New Simulation Approaches for Electronic Systems. Phys. Chem. Chem. Phys. 2015, 17, 31371–31396.

[63] Jensen, L.; Aikens, C. M.; Schatz, G. C. Electronic Structure Methods for Studying Surface-Enhanced Raman Scattering. Chem. Soc. Rev. 2008, 37, 1061–1073.

[64] Wu, K.; Chen, J.; McBride, J. R.; Lian, T. Efficient Hot-Electron Transfer by a Plasmon-Induced Interfacial Charge-Transfer Transition. Science 2015, 349, 632–635.

[65] Boerigter, C.; Campana, R.; Morabito, M.; Linic, S. Evidence and Implications of Direct Charge Excitation as the Dominant Mechanism in Plasmon-Mediated Photocatalysis. Nat. Comm. 2016, 7, 10545.

[66] Bernardi, M.; Mustafa, J.; Neaton, J. B.; Louie, S. G. Theory and Computation of Hot Carriers Generated by Surface Plasmon Polaritons in Noble Metals. Nat. Commun. 2015, 6, 7044.

[67] Sundararaman, R.; Narang, P.; Jermyn, A. S.; Goddard Iii, W. A.; Atwater, H. A. Theoretical Predictions for Hot-Carrier Generation from Surface Plasmon Decay. Nat. Commun. 2014, 5, 5788.

[68] Townsend, E.; Bryant, G. W. Plasmonic Properties of Metallic Nanoparticles: The Effects of Size Quantization. Nano Lett. 2012, 12, 429–434.

[69] Meng, Q.; May, P. S.; Berry, M. T.; Kilin, D. Sequential Hydrogen Dissociation from a Charged $Pt_{13}H_{24}$ Cluster Modeled by Ab Initio Molecular Dynamics. *Int. J. Quant. Chem.* **2012,**112, 3896–3903.

[70] Zhu, W.; Esteban, R.; Borisov, A. G.; Baumberg, J. J.; Nordlander, P.; Lezec, H. J.; Aizpurua, J.; Crozier, K. B. Quantum Mechanical Effects in Plasmonic Structures with Subnanometre Gaps. Nat. Comm. 2016, 7, 1–14.

[71] Wang, D.; Yang, A.; Wang, W.; Hua, Y.; Schaller, R. D.; Schatz, G. C.; Odom, T. W. Band-Edge Engineering for Controlled Multi-Modal Nanolasing in Plasmonic Superlattices. Nat. Nano. 2017, 12, 889–894.

[72] Harutyunyan, H.; Martinson, A. B. F.; Rosenmann, D.; Khorashad, L. K.; Besteiro, L. V.; Govorov, A. O.; Wiederrecht, G. P. Anomalous Ultrafast Dynamics of Hot Plasmonic Electrons in Nanostructures with Hot Spots. *Nat. Nano*. **2015**, 10, 770.

[73] Besteiro, L. V.; Govorov, A. O. Amplified Generation of Hot Electrons and Quantum Surface Effects in Nanoparticle Dimers with Plasmonic Hot Spots. *J. Phys. Chem. C* **2016**, 120, 19329–19339.

[74] Marinica, D.; Kazansky, A.; Nordlander, P.; Aizpurua, J.; Borisov, A. G. Quantum Plasmonics: Nonlinear Effects in the Field Enhancement of a Plasmonic Nanoparticle Dimer. *Nano Letters* **2012**, 12, 1333–1339.

[75] Cushing, S. K.; Li, J.; Bright, J.; Yost, B. T.; Zheng, P.; Bristow, A. D.; Wu, N. Controlling Plasmon-Induced Resonance Energy Transfer and Hot

Electron Injection Processes in Metal@TiO2 Core-Shell Nanoparticles. J. *Phys. Chem. C* **2015**, 119, 16239-16244.

[76] Sprague-Klein, E. A.; McAnally, M. O.; Zhdanov, D. V.; Zrimsek, A. B.; Apkarian, V. A.; Seideman, T.; Schatz, G. C.; Van Duyne, R. P. Observation of Single Molecule Plasmon-Driven Electron Transfer in Isotopically Edited 4,4'-Bipyridine Gold Nanosphere Oligomers. *J. Am. Chem. Soc*. **2017**, 139, 15212–15221.

[77] Galego, J.; Garcia-Vidal, F. J.; Feist, J. Suppressing Photochemical Reactions with Quantized Light Fields. *Nat. Comm.* **2016**, 7, 13841.

[78] Hutchison, J. A.; Schwartz, T.; Genet, C.; Devaux, E.; Ebbesen, T. W. Modifying Chemical Landscapes by Coupling to Vacuum Fields. *Angew. Chem. Int. Ed*. **2012**, 51, 1592–1596.

[79] Feist, J.; Galego, J.; Garcia-Vidal, F. J. Polaritonic Chemistry with Organic Molecules. *ACS Photonics* **2018**, 5, 205–216.

[80] Linic, S.; Christopher, P.; Ingram, D. Plasmonic-metal nanostructures for efficient conversion of solar to chemical energy. *Nat. Mater.* **2011**, 10, 911-921.

[81] , J.; Wu, J.; Wu, P.; Tsai, D. Plasmonic Photocatalyst for $H_2$ Evolution in Photocatalytic Water Splitting. *J. Phys. Chem. C* **2011**, 115, 210-216.

[82] Priebe, J. B.; Karnahl, M.; Junge, H.; Beller, M.; Hollmann, D.; Bruckner, A. Water Reduction with Visible Light: Synergy between Optical Transitions and Electron Transfer in Au-$TiO_2$ Catalysts Visualized by In situ EPR Spectroscopy. *Angew. Chem. Int. Ed.* **2013**, 52, 11420 –11424.